EDGE ARTICLE

Comparative study of CO_2 insertion into pincer supported palladium alkyl and aryl complexes†

Anthony P. Deziel,[a] Sahil Gahlawat,[bc] Nilay Hazari,[*a] Kathrin H. Hopmann[*b] and Brandon Q. Mercado[a]

The insertion of CO_2 into metal alkyl bonds is a crucial elementary step in transition metal-catalyzed processes for CO_2 utilization. Here, we synthesize pincer-supported palladium complexes of the type (^{tBu}PBP)Pd(alkyl) (^{tBu}PBP = $B(NCH_2P^tBu_2)_2C_6H_4^-$; alkyl = CH_2CH_3, $CH_2CH_2CH_3$, $CH_2C_6H_5$, and CH_2-4-OMe-C_6H_4) and (^{tBu}PBP)Pd(C_6H_5) and compare the rates of CO_2 insertion into the palladium alkyl bonds to form metal carboxylate complexes. Although, the rate constant for CO_2 insertion into (^{tBu}PBP)Pd(CH_2CH_3) is more than double the rate constant we previously measured for insertion into the palladium methyl complex (^{tBu}PBP)Pd(CH_3), insertion into (^{tBu}PBP)Pd($CH_2CH_2CH_3$) occurs approximately one order of magnitude slower than (^{tBu}PBP)Pd(CH_3). CO_2 insertion into the benzyl complexes (^{tBu}PBP)Pd($CH_2C_6H_5$) and (^{tBu}PBP)Pd(CH_2-4-OMe-C_6H_4) is significantly slower than any of the n-alkyl complexes, and CO_2 does not insert into the palladium phenyl bond of (^{tBu}PBP)Pd(C_6H_5). While (^{tBu}PBP)Pd(CH_2CH_3) and (^{tBu}PBP)Pd($CH_2CH_2CH_3$) are resistant to β-hydride elimination, we were unable to synthesize complexes with *n*-butyl, *iso*-propyl, and *tert*-butyl ligands due to β-hydride elimination and an unusual reductive coupling, which involves the formation of new C−B bonds. This reductive process also occurred for (^{tBu}PBP)Pd($CH_2C_6H_5$) at elevated temperature and a related process involving the formation of a new H−B bond prevented the isolation of (^{tBu}PBP)PdH. DFT calculations provide insight into the relative rates of CO_2 insertion and indicate that steric factors are critical. Overall, this work is one of the first comparative studies of the rates of CO_2 insertion into different metal alkyl bonds and provides fundamental information that may be important for the development of new catalysts for CO_2 utilization.

Introduction

There is considerable interest in the use of carbon dioxide (CO_2) as a carbon containing chemical feedstock due to its low cost, non-toxic nature, and abundance.[1] However, only a small number of chemicals are currently industrially produced from CO_2.[1g] This is in part because the kinetic barriers associated with bond forming processes involving CO_2 are often prohibitively high. Transition metal catalysts represent a promising method to increase the range of products generated from CO_2 because they can create lower energy pathways for activating and functionalizing CO_2.[1] To date, most transition metal catalysts for CO_2 utilization have converted CO_2 into other C_1 products such as methane, CO, formic acid, and methanol and there are limited examples of catalysts that can form products containing C–C bonds, such as fuels, from CO_2.[1g] As a result, the formation of products containing a C–C bond from CO_2 has been identified as a high priority research area by the United States National Academies of Science.[2]

$$L_nM—E \xrightarrow{CO_2} L_nM—O—C(=O)—E \quad (1)$$
E = H, OR, NR_2, or CR_3
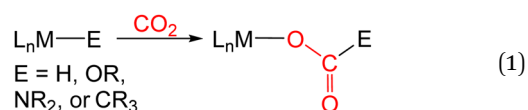
In many transition metal catalyzed processes for CO_2 utilization, the insertion of CO_2 into a metal–E σ-bond (for example E = H, OR, NR_2, or CR_3) is a crucial elementary step (eqn (1)).[3] This is especially the case for late transition metals, where the relative weakness of the M–O bonds makes subsequent cleavage of the M–O bond more facile.[3] The insertion of CO_2 into a metal alkyl bond is a particularly important reaction because it can ultimately result in the generation of products containing a C–C bond. For example, Group 10 catalysts have been used for the formation of carboxylic acids through the carboxylation of

[a]Department of Chemistry, Yale University, P. O. Box 208107, New Haven, Connecticut, 06520, USA. E-mail: nilay.hazari@yale.edu

[b]Department of Chemistry, UiT The Arctic University of Norway, N-9307 Tromsø, Norway. E-mail: kathrin.hopmann@uit.no

[c]Hylleraas Center for Quantum Molecular Sciences, UiT The Arctic University of Norway, 9037 Tromsø, Norway

a variety of alkyl halides and pseudo halides.[4] In these reactions, C–C bonds are proposed to form between CO_2 and the alkyl electrophile *via* the insertion of CO_2 into a metal alkyl bond. However, at this stage there is limited experimental information on the pathways for CO_2 insertion into metal alkyl bonds, as most studies have primarily involved isolated examples with a single metal complex,[5–14] and thus, it is unclear how changing the nature of the alkyl group or ancillary ligand impacts the reaction. Further, kinetic studies are relatively rare,[6,8a,b,9d,11c,13g,14b] which means that computational results cannot be benchmarked against experimental data.

Previous kinetic studies exploring CO_2 insertion into well-defined metal alkyl complexes have almost exclusively focused on metal methyl species.[6,8a,b,9d,11c,13g,14b] This is because of the stability of metal methyl complexes, which in contrast to longer chain alkyl containing complexes, such as metal ethyl complexes, do not undergo β-hydride elimination. A major limitation in studying CO_2 insertion into metal methyl bonds, and in particular the types of Group 10 metal alkyl complexes that are relevant to catalysis, is the paucity of systems that are stable and react under mild reaction conditions. Most systems require high temperatures and do not give quantitative yields of products, which prevents kinetic studies. We recently described the insertion of CO_2 into palladium and nickel methyl complexes supported by ^{R}PBP ($^{R}PBP = B(NCH_2PR_2)_2C_6H_4^{-}$; R = Cy or ^{t}Bu) pincer ligands (Fig. 1a).[13g] The strong *trans*-influence of the boryl donor in the pincer ligand destabilizes the methyl group and as a consequence these complexes insert CO_2 at room temperature, which enabled us to perform detailed kinetic studies on CO_2 insertion into a metal methyl bond.

We hypothesized that the ^{R}PBP framework may stabilize palladium complexes with other alkyl ligands, as pincer ligands are known to inhibit β-hydride elimination from square planar palladium(II) complexes.[15] Further, given that the ^{R}PBP ligand can facilitate CO_2 insertion reactions under mild conditions,[13g] we postulated that the synthesis of a family of ^{R}PBP supported palladium alkyl complexes would enable us to perform a rare experimental comparison of the rates of CO_2 insertion as the alkyl ligand is varied. In this work, we describe the synthesis of a series of ^{tBu}PBP supported palladium complexes with ethyl, n-propyl, benzyl, and phenyl ligands. Although $(^{tBu}PBP)Pd(CH_2-CH_3)$ (**1-Et**), $(^{tBu}PBP)Pd(CH_2CH_2CH_3)$ (**1-^{n}Pr**), (^{tBu}PBP) PdCH$_2$C$_6$H$_5$ (**1-Bn**), and $(^{tBu}PBP)PdCH_2$-4-OMe-C$_6$H$_4$ (**1-^{OMe}Bn**), are sufficiently stable in solution to be isolated, attempts to synthesize complexes with n-butyl, iso-propyl, and tert-butyl ligands were unsuccessful due to rapid decomposition *via* either β-hydride elimination or an unusual reductive pathway that generates a new C–B bond. A similar reductive process to form a new H–B bond occurs in the putative hydride complex $(^{tBu}PBP)PdH$. The stability of **1-Et**, **1-^{n}Pr**, **1-Bn**, and **1-^{OMe}Bn** allowed us to determine the rates of CO_2 insertion into the palladium alkyl bonds. The rate constant for CO_2 insertion into **1-Et** is *over double* the rate constant previously measured for CO_2 insertion into $(^{tBu}PBP)Pd(CH_3)$ (**1-Me**),[13g] while insertion into **1-^{n}Pr** occurs at *approximately one-tenth* the rate of **1-Me**. This is a remarkable difference given the relatively minor changes in the alkyl ligand. The insertion of CO_2 into the benzyl complexes, **1-Bn** and **1-^{OMe}Bn**, is significantly slower than any of n-alkyl complexes and CO_2 does not insert into the palladium phenyl bond of the related complex $(^{tBu}PBP)Pd(C_6H_5)$ (**1-Ph**). DFT calculations enabled the rationalization of the relative rates of CO_2 insertion and suggest that steric factors are the predominant reason for the differences in the rates of insertion between **1-Me**, **1-Et**, and **1-^{n}Pr**. Overall, the fundamental insight on CO_2 insertion provided in this work will likely assist in the development of improved and new catalysts for CO_2 utilization.

Results and discussion

Synthesis of ^{tBu}PBP supported palladium alkyl and aryl complexes

Previous studies have demonstrated that reactions of complexes of the form $(^{R}PBP)PdCl$ (R = ^{i}Pr or ^{t}Bu) with MeLi generate stable palladium methyl complexes.[13g] In an analogous fashion, treatment of $(^{tBu}PBP)PdCl$ (**1-Cl**) with EtLi or $^{n}PrMgCl$ in benzene results in the formation of $(^{tBu}PBP)Pd(CH_2CH_3)$ (**1-Et**) and $(^{tBu}PBP)Pd(CH_2CH_2CH_3)$ (**1-^{n}Pr**), which were isolated in yields of 76 and 59%, respectively, after recrystallization (eqn (2)).[16] **1-Et** is a rare example of an isolated pincer supported palladium ethyl complex,[15,17] while **1-^{n}Pr** is to the best of our knowledge only the second example of an isolated palladium propyl complex.[18] **1-Et** and **1-^{n}Pr** are indefinitely stable at room temperature in benzene and β-hydride elimination to generate ethylene or propene and a putative palladium hydride (*vide*
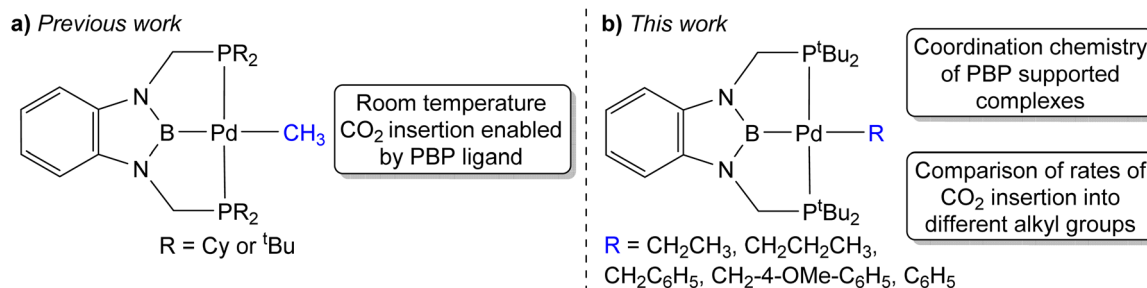

Fig. 1 (a) Previous example of CO_2 insertion into ^{R}PBP supported palladium methyl complexes at room temperature. (b) ^{tBu}PBP supported palladium complexes studied in this work, which reveal fundamental information about the coordination chemistry of the ^{tBu}PBP ligand and enable a comparison between the rates of CO_2 insertion as a function of the alkyl ligand.
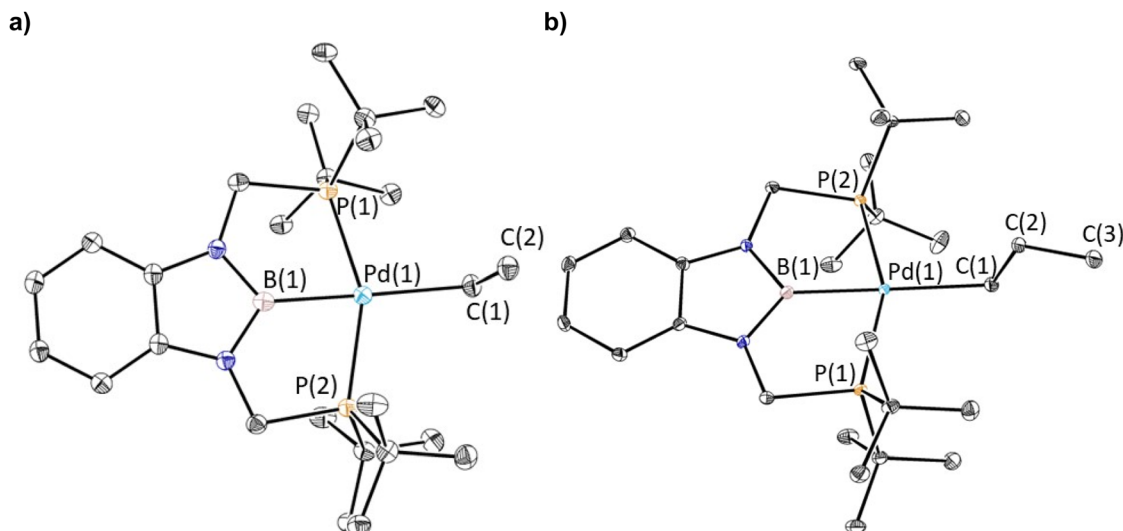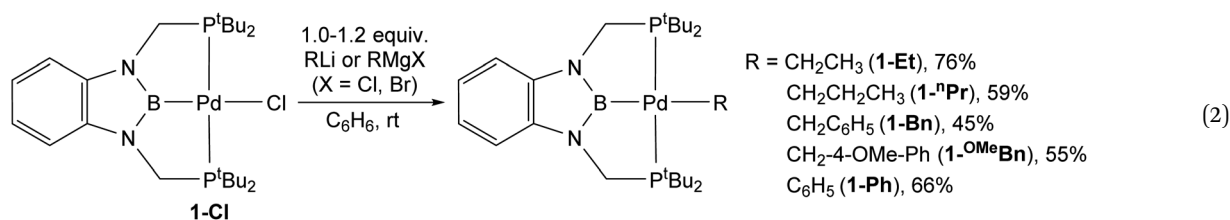
a)

b)

Fig. 2 (a) Solid-state structure of **1-Et** with thermal ellipsoids at 30% probability. Hydrogen atoms are omitted for clarity. Selected distances (Å) and angles (°): Pd(1)–B(1) 2.029(7), Pd(1)–C(1) 2.226(6), Pd(1)–P(1) 2.3184(15), Pd(1)–P(2) 2.3189(14), C(1)–C(2) 1.506(9), B(1)–Pd(1)–C(1) 175.3(2), B(1)–Pd(1)–P(1) 76.39(19), B(1)–Pd(1)–P(2) 78.23(19), C(1)–Pd(1)–P(1) 103.15(18), C(1)–Pd(1)–P(2) 102.61(18), P(1)–Pd(1)–P(2) 153.99(6), Pd(1)–C(1)–C(2) 115.8(4). (b) Solid-state structure of **1-^{n}Pr** with thermal ellipsoids at 30% probability. Hydrogen atoms are omitted for clarity. Selected distances (Å) and angles (°): Pd(1)–B(1) 2.020(3), Pd(1)–C(1) 2.209(2), Pd(1)–P(1) 2.3143(5), Pd(1)–P(2) 2.3135(5), C(1)–C(2) 1.531(3), C(2)–C(3) 1.528(3), P(1)–Pd(1)–P(2) 154.23(2), C(1)–Pd(1)–P(1) 101.54(6), C(1)–Pd(1)–P(2) 103.95(6), B(1)–Pd(1)–P(1) 77.67(7), B(1)–Pd(1)–P(2) 77.07(7), B(1)–Pd(1)–C(1) 177.01(9), Pd(1)–C(1)–C(2) 114.49(15).

infra) only occurs at temperatures greater than 60 °C. Recrystallization from pentane generated crystals of **1-Et** and **1-^{n}Pr** suitable for X-ray diffraction (Fig. 2a and b). In both cases, the geometry around Pd is distorted square planar and the P(1)–Pd(1)–P(2) bond angles are 153.99(6) and 154.23(2)° in **1-Et** and **1-^{n}Pr**, respectively, indicating that the phosphorus donors of the pincer ligand deviate significantly from linearity. The Pd–B bond distances are 2.029(7) Å in **1-Et** and 2.020(3) Å in **1-^{n}Pr**, which are significantly longer than the Pd–B bond distance in (^{tBu}PBP)PdCl (Pd–B is 1.972(4) Å in **1-Cl**).[19] This is consistent with the ethyl or propyl ligand exerting a stronger *trans*-

tetrahedral in both **1-Et** and **1-^{n}Pr** and Pd(1)–C(1)–C(2) angles of 115.8(4)° and 114.49(15)°, respectively, are observed. Analysis of the literature reveals that this is a general trend for Group 10 alkyl complexes.[21] Overall, the geometrical parameters around palladium are similar in **1-Me**,[13g] **1-Et**, and **1-^{n}Pr**, with the exception that the Pd–C bond distance in **1-Me** is slightly shorter than in **1-Et** or **1-^{n}Pr** (Pd(1)–C(1) is 2.185(4) Å in **1-Me**), which is qualitatively consistent with DFT calculations (*vide infra*). This suggests that as expected the change from methyl to ethyl to *n*-propyl has little impact on the geometry around palladium.

R = CH$_2$CH$_3$ (**1-Et**), 76%
CH$_2$CH$_2$CH$_3$ (**1-^{n}Pr**), 59%
CH$_2$C$_6$H$_5$ (**1-Bn**), 45%
CH$_2$-4-OMe-Ph (**1-^{OMe}Bn**), 55%
C$_6$H$_5$ (**1-Ph**), 66%

(2)

influence than a chloride ligand. Although, crystallographically characterized examples of palladium ethyl complexes are rare,[15,17,20] the Pd–C bond distance in **1-Et** is longer than those typically reported (Pd(1)–C(1) is 2.226(6) Å in **1-Et**) and is most comparable to a PSiP-supported palladium ethyl complex, which also contains a strong *trans*-influence donor (silyl) opposite the palladium.[15] In **1-^{n}Pr** the Pd(1)–C(1) is 2.209(2) Å, which is within error of the Pd–C bond distance in **1-Et**. The carbon atom bound to palladium (C(1)) is distorted from

The reaction of **1-Cl** with (CH$_2$C$_6$H$_5$)MgCl or (4-OMe-CH$_2$C$_6$H$_4$)MgCl resulted in the isolation of **1-Bn** or **1-^{OMe}Bn**, which are rare examples of pincer supported benzyl complexes,[22] in yields of 45% or 55%, respectively (eqn (2)). In both cases, it is important to remove the MgCl$_2$ by-product from the Grignard reagent or the benzyl complexes slowly convert back to **1-Cl** in solution. In fact, the relatively low yields of **1-Bn** and **1-^{OMe}Bn** are in part due to the successive recrystallizations that are required to ensure MgCl$_2$ impurities are not present.

Both **1-Bn** and **1-OMeBn** were characterized by X-ray crystallography (Fig. 3a and b). The solid-state structures indicate that the geometry around palladium is distorted square planar and the geometrical parameters associated with the binding of the tBuPBP ligand in **1-Bn** and **1-OMeBn** are analogous to those in **1-Et** and **1-nPr**. The long Pd–B bond distances (2.032(4) Å in **1-Bn** and 2.025(3) Å in **1-OMeBn**) are consistent with the high *trans*-influence of the benzyl ligand. The benzyl ligand binds in an η^1-fashion with Pd–C bond distances of 2.260(3) Å in **1-Bn** and 2.249(3) Å in **1-OMeBn**, which are longer than almost all other palladium complexes that feature an η^1-benzyl ligand.[22] Further, the carbon atom bound to palladium (C(1)) is significantly distorted from tetrahedral, with Pd(1)–C(1)–C(2) angles of 127.7(2)° and 123.44(18)° observed for **1-Bn** and **1-OMeBn**, respectively. Although this deviation from tetrahedral is typical for Group 10 benzyl complexes,[21a,c,23] these are some of the largest angles reported perhaps due to the steric congestion around the palladium.

1-Bn is stable when left in C_6D_6 at room temperature, but complete decomposition is observed when it is heated for 3 days at 65 °C, with the major product being a new dimeric complex, (tBuPBBnP)$_2$Pd$_2$ (**2-Bn**, Bn = benzyl) (Fig. 4a). Based on NMR spectroscopy we propose that **1-OMeBn** decomposes *via* a similar pathway (see ESI†). **2-Bn** was characterized by X-ray crystallography (Fig. 4b). In **2-Bn**, two new C–B bonds have formed presumably due to a reductive coupling reaction between the benzyl ligands and the boron atom of the tBuPBP ligands. This causes a reduction in the palladium center from palladium(II) in **1-Bn** to palladium(0) in **2-Bn**. The boron atom of the pincer ligand no longer coordinates to the palladium center and the two phosphorus donors of the new bidentate tBuPBBnP ligands do not coordinate to the same palladium center but instead coordinate to two different palladium atoms. The pathway for this ligand rearrangement is unclear. Consistent with the reduction in oxidation state, the geometry around the palladium centers in **2-Bn** are distorted linear. We have previously observed a similar decomposition pathway for (tBuPBP)Ni(CH$_3$), which results in the formation of a nickel(0) dinitrogen complex,[13g] but this is the first time the reductive decomposition pathway has been observed for palladium. We hypothesize that reductive coupling occurs more readily in **1-Bn** compared to **1-Et** or **1-Me** (where it is not observed to any significant extent spectroscopically) because there is greater steric congestion in the case of the palladium benzyl complex. This is also in agreement with the observation of reductive coupling in the case of (tBuPBP)Ni(CH$_3$) but not **1-Me**, as the smaller nickel center presumably results in a more congested metal center.[13g] Our results suggest that C–B bond formation is potentially a general decomposition pathway for RPBP supported complexes, rather than a curiosity that is only relevant to a single complex.

Although the reaction between **1-Cl** and EtLi results in clean formation of **1-Et**, the corresponding reactions between **1-Cl** and nBuLi, iPrLi, and tBuMgCl did not result in the generation of isolable palladium alkyl complexes and instead various decomposition products are observed (Table 1).[24,25] In the case of tBuMgCl, the initial metathesis reaction is slow and even after three days at room temperature some **1-Cl** is still present, along with three new peaks in the ^{31}P NMR spectra. Although we do not observe (tBuPBP)Pd(tBu) (**1-tBu**) directly, the peaks observed are consistent with the formation and decomposition of (tBuPBP)PdH (**1-H**) (*vide infra* and see ESI†). **1-H** presumably forms *via* β-hydride elimination from **1-tBu** and in agreement with this proposal iso-butene is observed by ^{1}H NMR spectroscopy. This suggests that **1-tBu** is unstable at room temperature
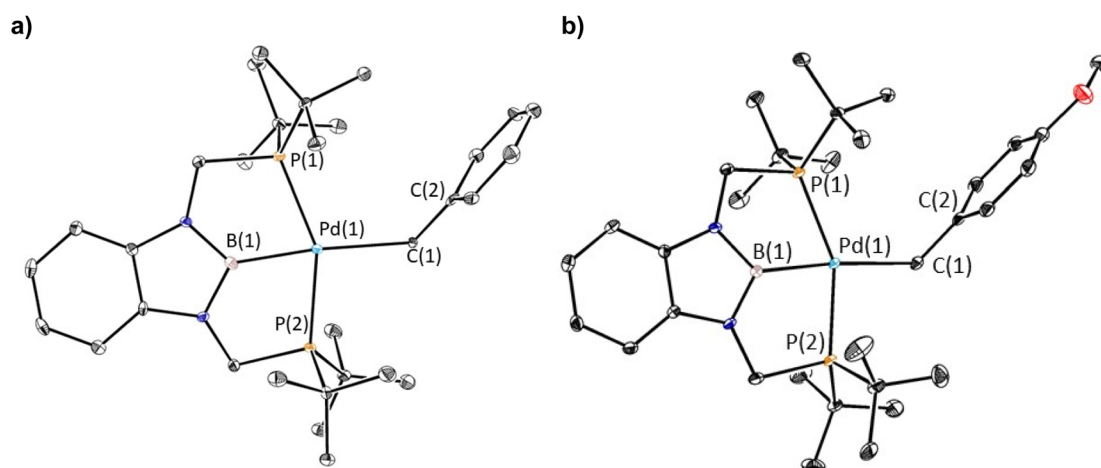

Fig. 3 (a) Solid-state structure of **1-Bn** with thermal ellipsoids at 30% probability. Hydrogen atoms are omitted for clarity. Selected distances (Å) and angles (°): Pd(1)–B(1) 2.032(4), Pd(1)–C(1) 2.260(3), Pd(1)–P(1) 2.3429(10), Pd(1)–P(2) 2.3407(10), C(1)–C(2) 1.477(5), B(1)–Pd(1)–C(1) 174.32(15), B(1)–Pd(1)–P(1) 76.60(12), B(1)–Pd(1)–P(2) 77.27(12), C(1)–Pd(1)–P(1) 108.72(9), C(1)–Pd(1)–P(2) 97.33(9), P(1)–Pd(1)–P(2) 153.77(3), Pd(1)–C(1)–C(2) 127.7(2). (b) Solid-state structure of **1-OMeBn** with thermal ellipsoids at 30% probability. Hydrogen atoms are omitted for clarity. Selected distances (Å) and angles (°): Pd(1)–B(1) 2.025(3), Pd(1)–C(1) 2.249(3), Pd(1)–P(1) 2.3360(7), Pd(1)–P(2) 2.3402(8), C(1)–C(2) 1.486(4), P(1)–Pd(1)–P(2) 154.50(3), C(1)–Pd(1)–P(1) 107.42(8), C(1)–Pd(1)–P(2) 97.83(7), B(1)–Pd(1)–P(1) 77.05(9), B(1)–Pd(1)–P(2) 77.53(9), B(1)–Pd(1)–C(1) 174.21(11), Pd(1)–C(1)–C(2) 123.44(18).
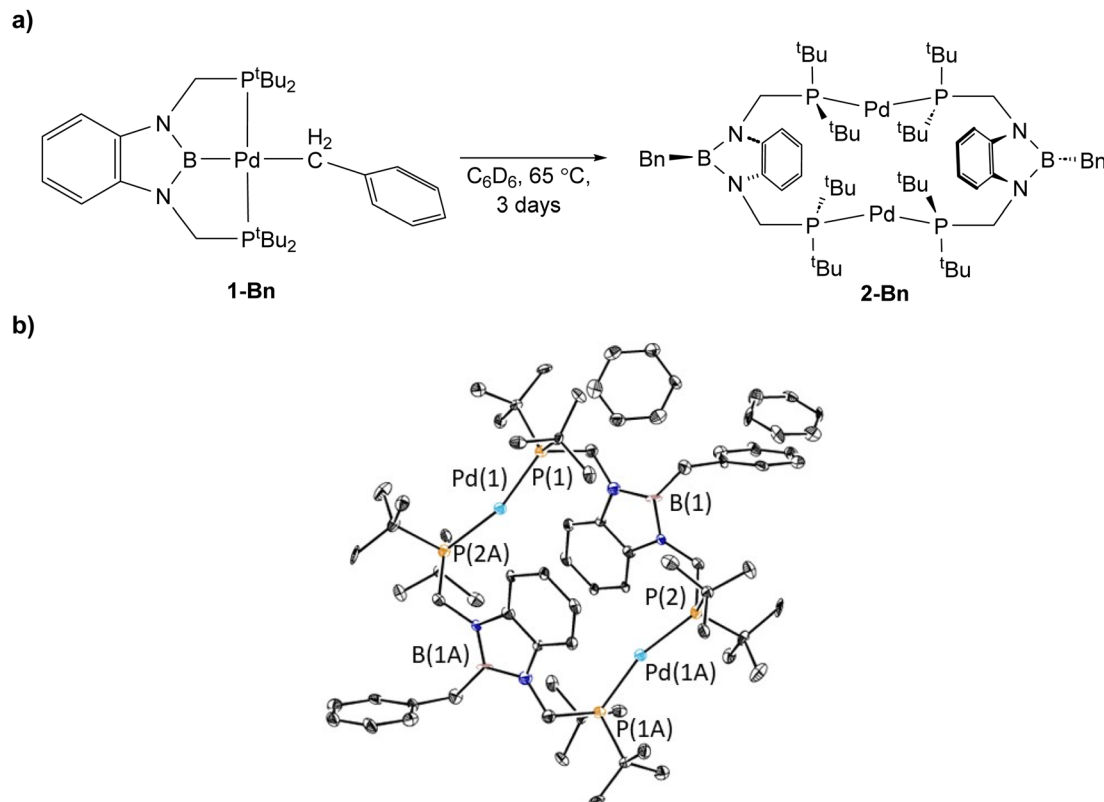
Fig. 4 (a) Reaction scheme for decomposition of (^{tBu}PBP)Pd(CH$_2$C$_6$H$_5$) (**1-Bn**) to (^{tBu}PB^{Bn}P)$_2$Pd$_2$ (**2-Bn**) and (b) solid-state structure of **2-Bn** with thermal ellipsoids at 30% probability. Hydrogen atoms are omitted for clarity. Selected distances (Å) and angles (°): Pd(1)−P(1) 2.277(2), Pd(1)−P(2A) 2.273(2), P(1)−Pd(1)−P(2A) 163.34(9).

and performing the reaction at low temperature is not possible due to the slow rate of the initial metathesis reaction.

The reaction between **1-Cl** and ^{i}PrLi is rapid and after 10 minutes at room temperature there is no **1-Cl** left in the reaction mixture. At this time, one major peak is observed in the ^{31}P NMR spectrum at 15.6 ppm, which based on its downfield chemical shift is unlikely to be (^{tBu}PBP)Pd(^{i}Pr) (**1-^{i}Pr**). Typically, palladium(ii) complexes containing a ^{tBu}PBP ligand have chemical shifts between 60–120 ppm, whereas the chemical shift of the free ^{tBu}PB^{H}P ligand is 17.0 ppm.[26] There is also no evidence for the generation of products associated with β-hydride elimination from **1-^{i}Pr**, as no signals corresponding to (^{tBu}PBP)PdH (**1-H**) (or related decomposition products, *vide infra*) are observed in the ^{1}H or ^{31}P NMR spectra, and there are no resonances associated with propene in the ^{1}H NMR spectrum. Instead, we propose that the major species in the ^{31}P NMR spectrum is the organic compound ^{tBu}PB^{iPr}P, which was confirmed by mass spectrometry (see ESI†). We propose that ^{tBu}PB^{iPr}P forms from the rapid reductive decomposition of **1-^{i}Pr**, which is generated but not observed in the reaction. The reductive process that **1-^{i}Pr** is postulated to undergo is akin to what we observed in the decomposition of **1-Bn** (*vide supra*) in that a new C–B bond is formed. However, in the case of **1-^{i}Pr**, we only see the free organic product ^{tBu}PB^{iPr}P and there is no evidence that ^{tBu}PB^{iPr}P coordinates to palladium to form a dimer analogous to **2-Bn**. Instead, palladium black

precipitates out of solution. At this stage, it is unclear why ^{tBu}PB^{iPr}P does not coordinate to palladium in a similar fashion to ^{tBu}PB^{Bn}P, and it is possible although unlikely that ^{tBu}PB^{iPr}P is formed through a pathway that does not even involve the formation of **1-^{i}Pr**.

The reaction between **1-Cl** and ^{n}BuLi proceeds in an analogous fashion to the reaction between **1-Cl** and ^{i}PrLi and ultimately gives palladium black and ^{tBu}PB^{nBu}P. However, the proposed intermediate alkyl complex, (^{tBu}PBP)Pd(^{n}Bu) (**1-^{n}Bu**), is more stable and at −35 °C the reaction mixture contained primarily **1-^{n}Bu** (∼97%), with only a small amount of the organic decomposition product ^{tBu}PB^{nBu}P (∼3%) (see ESI†). Heating the sample to room temperature resulted in an increase in the amount of decomposition product and it was not possible to isolate **1-^{n}Bu**. In contrast, as described above, it is possible to cleanly isolate **1-^{n}Pr** from the reaction between **1-Cl** and ^{n}PrMgCl and decomposition of **1-^{n}Pr** only occurs at 60 °C (eqn (2)). In this case, propene is observed in the ^{1}H NMR spectra along with products consistent with the formation and decomposition of **1-H** (*vide infra*), suggesting that decomposition primarily occurs *via* β-hydride elimination. Similar decomposition *via* β-hydride elimination is observed at 65 °C for **1-Et**, with ethylene observed as a by-product. We also examined the stability of previously reported **1-Me**[13g] and demonstrated that at 65 °C it undergoes very slow C–B reductive coupling to form (^{tBu}PB^{Me}P)$_2$Pd$_2$ (**2-Me**) (see ESI†). Our results

Table 1 Summary of the reactions of RMgCl or RLi with ($^{t\mathrm{Bu}}$PBP)PdCl (**1-Cl**)
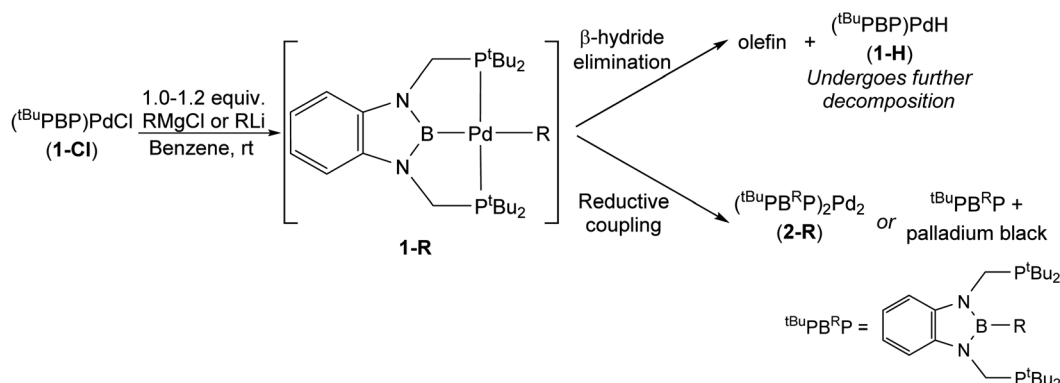
Entry	Reagent	**1-R** isolable	Stability of **1-R** at rt	Decomposition pathway
1	MeLi	Yes[a]	Stable[a]	Slow reductive coupling (at 65 °C) to give **2-Me** (see ESI)
2	EtLi	Yes	Stable	β-Hydride elimination (at 65 °C)
3	^{n}PrMgCl	Yes	Stable	β-Hydride elimination (at 65 °C)
4	^{n}BuLi	No	Unstable	Reductive coupling to give $^{t\mathrm{Bu}}$PB$^{n\mathrm{Bu}}$P and palladium black
5	^{i}PrLi	No	Not observed	Reductive coupling to give $^{t\mathrm{Bu}}$PB$^{i\mathrm{Pr}}$P and palladium black
6	^{t}BuMgCl	No	Not observed	β-Hydride elimination
7	BenzylMgCl	Yes	Stable	Reductive coupling (at 65 °C) to give **2-Bn**
8	4-OMe-BenzylMgCl	Yes	Stable	Reductive coupling (at 65 °C) to give **2-$^{\mathrm{OMe}}$Bn**[b]

[a] See ref. 13g. [b] **2-$^{\mathrm{OMe}}$Bn** was characterized by analogy to **2-Bn** and was not isolated.

indicate that the stability of $^{t\mathrm{Bu}}$PBP ligated Pd alkyl complexes is related to the steric bulk of the alkyl group, so the order of stability is **1-^{t}Bu** ~ **1-^{i}Pr** < **1-^{n}Bu** < **1-^{n}Pr** ~ **1-Et** < **1-Me**. Interestingly, the least and most sterically bulky complexes decompose *via* β-hydride elimination, while those with intermediate steric properties decompose through reductive coupling. **1-Me** is an exception as it lacks any β-hydrogens and therefore despite its small size decomposes *via* reductive coupling.

To verify our hypothesis that the rapid decomposition of **1-^{t}Bu** results in the formation of the palladium hydride complex **1-H**, we attempted to independently prepare **1-H**. Reaction of **1-Cl** with 1 equivalent of LiHBEt$_3$ in C$_6$D$_6$ generated two major products in an approximately 55 : 45 ratio by ^{1}H and ^{31}P NMR spectroscopy (Fig. 5). We propose that one of these is **1-H** because the ^{31}P NMR chemical shift (115 ppm, 55%) is very close to the shift for the corresponding ($^{t\mathrm{Bu}}$PBP)PtH complex (114.5 ppm).[27] The other resonance in the ^{31}P NMR spectra is observed at 96.4 ppm, but even though it is present in both the decomposition of **1-^{t}Bu**, **1-Et**, and **1-^{n}Pr**, as well as the attempted direct synthesis of **1-H**, we are unsure of the identity of the complex giving rise to this signal. Further, although the complex giving rise to the signal at 96.4 ppm is relatively stable over 12 hours, the complex giving rise to the signal at 115 ppm decomposes at room temperature in C$_6$D$_6$ to give a dimeric palladium(0) complex, **2-H**, in which the hydride has reductively coupled with the boron atom of the $^{t\mathrm{Bu}}$PBP ligand to give a new H–B bond (Fig. 5). This is an analogous process to the decomposition of **1-Bn**, except an H–B bond is formed instead of a C–B bond. **2-H** was characterized by single crystal X-ray diffraction

(Fig. 5b) and contains two distorted linear palladium(0) centers. The phosphorous atoms of the pincer ligands have rearranged so they bind to two different palladium centers rather than a single palladium center. In this case, it is presumably not steric factors that drive the decomposition of the palladium hydride but the formation of a strong H–B bond. Given the large number of stable pincer-supported palladium hydrides,[28] we hypothesize that **1-H** is unstable because of the *trans*-influence of the boryl ligand, which significantly destabilizes the hydride relative to other species which have weaker *trans*-influence ligands opposite the hydride.

To compare the reactivity of $^{t\mathrm{Bu}}$PBP supported palladium alkyl complexes with a $^{t\mathrm{Bu}}$PBP supported palladium aryl species, we prepared ($^{t\mathrm{Bu}}$PBP)Pd(C$_6$H$_5$) (**1-Ph**) (eqn (2)). Although, the synthesis of **1-Ph** followed the same route as the palladium alkyl species described above,[29] the reaction of **1-Cl** with PhMgBr was significantly slower than the corresponding reactions with alkyl lithium or Grignard reagents. Specifically, the reaction with PhMgBr took two days to reach completion at room temperature, whereas the reactions with alkyl lithium or Grignard reagents were typically complete in less than one hour at room temperature (except for ^{t}BuMgCl). This is likely related to the lower nucleophilicity of aryl Grignard reagents compared with alkyl Grignard reagents. After recrystallization to remove Mg salt impurities, we were able to isolate **1-Ph** in 66% yield. **1-Ph** was characterized by X-ray crystallography (see ESI†). The Pd–C bond distance in is 2.162(3) Å, which is significantly shorter than the Pd–C bond length in all of our palladium alkyl complexes. This is likely due to the fact that the carbon atom
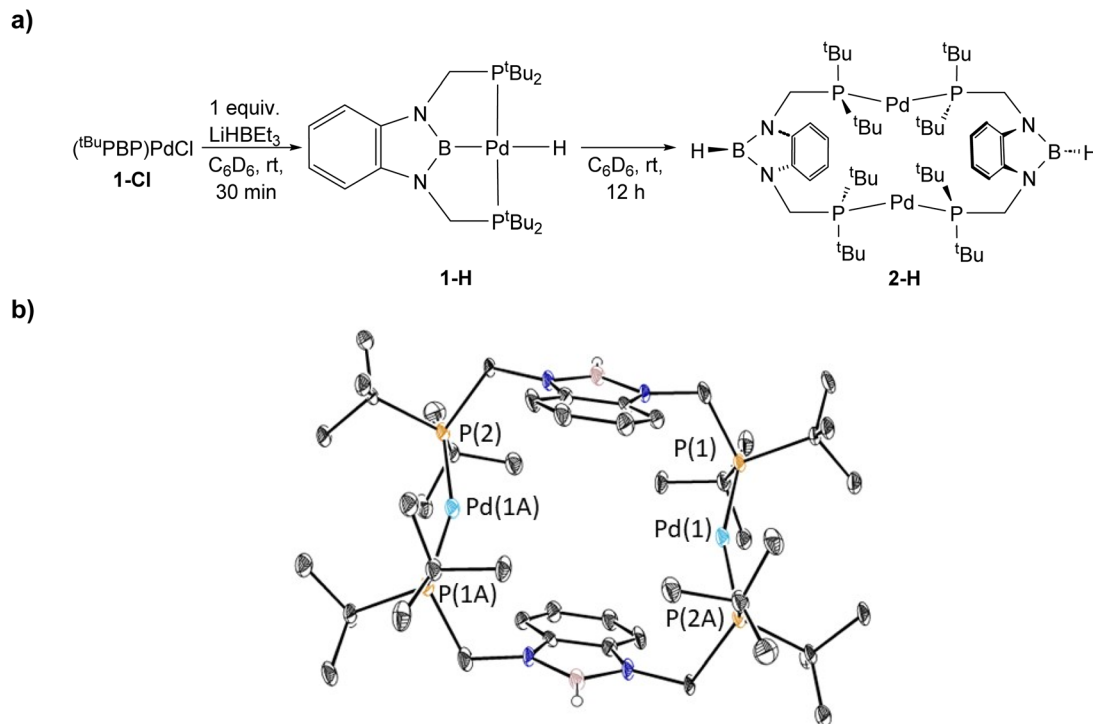
a)

b)

Fig. 5 (a) Synthesis and decomposition of ^{tBu}PBP supported palladium hydride, **1-H**, to form (^{tBu}PB^{H}P)$_2$Pd$_2$ (**2-H**). The decomposition at room temperature in solution prevented the isolated of **1-H**. (b) Solid-state structure of **2-H** with thermal ellipsoids at 30% probability. Hydrogen atoms are omitted for clarity. Selected distances (Å) and angles (°): Pd(1)−P(1) 2.2821(15), Pd(1)−P(2A) 2.2850(15), P(1)−Pd(1)−P(2A) 159.99(5).

bound to palladium in **1-Ph** is sp^2-hybridized and is consistent with the trend observed for PCP-supported pincer complexes.[14]

Reactivity of ^{tBu}PBP supported palladium alkyl and aryl complexes with CO_2

The reaction of **1-Et** with 1 atm of CO_2 in C$_6$D$_6$ at room temperature quantitively generated the palladium carboxylate complex (^{tBu}PBP)Pd{OC(O)CH$_2$CH$_3$} (**3-Et**) in approximately 2 hours (Fig. 6). This is the fastest rate of CO_2 insertion observed for a pincer supported palladium alkyl species. **3-Et** was isolated and characterized using single crystal X-ray diffraction (Fig. 7). The solid-state structure confirms κ^1-binding of the carboxylate. The Pd–O bond distance is 2.1803(14) Å, which is relatively long for a palladium(II) carboxylate complex.[13g,14a,30] This suggests that it will be easier to cleave the Pd–O bond in **3-Et** compared to related palladium carboxylate complexes, which have been

generated *via* CO_2 insertion reactions.[6,14a] The Pd–B bond distance is significantly shorter in **3-Et** (1.973(2) Å) compared with **1-Et** (2.029(7) Å), which is consistent with the carboxylate ligand exerting a significantly weaker *trans*-influence than the ethyl ligand.
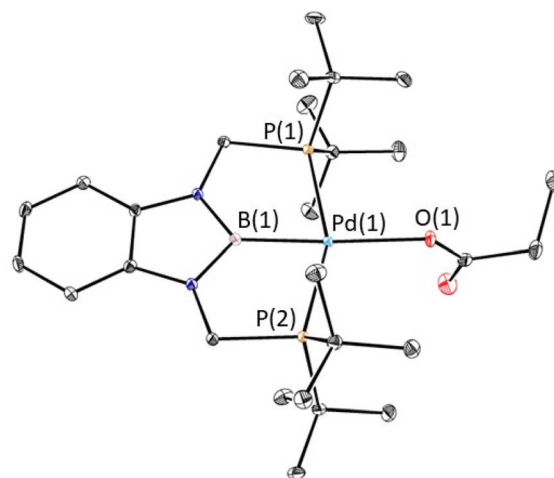
Fig. 7 Solid-state structure of **3-Et** with thermal ellipsoids at 30% probability. Hydrogen atoms are omitted for clarity. Selected distances (Å) and angles (°): Pd(1)−B(1) 1.973(2), Pd(1)−O(1) 2.1803(14), Pd(1)−P(1) 2.3449(5), Pd(1)−P(2) 2.3450(5), B(1)−Pd(1)−O(1) 173.80(7), B(1)−Pd(1)−P(1) 78.20(7), B(1)−Pd(1)−P(2) 78.45(7), O(1)−Pd(1)−P(1) 101.78(4), O(1)−Pd(1)−P(2) 101.30(4), P(1)−Pd(1)−P(2) 156.617(19), Pd(1)−O(1)−C(1) 123.46(14).

R = CH$_2$CH$_3$; >99% conversion after 2 hours; quantitative
R = CH$_2$CH$_2$CH$_3$; >99% conversion after 3 days; quantitative
R = CH$_2$C$_6$H$_5$; >99% conversion after 5 days; quantitative
R = CH$_2$-4-OMe-C$_6$H$_4$; >99% conversion after 5 days; quantitative

Fig. 6 Relative rates of CO_2 insertion into ^{tBu}PBP supported palladium alkyl complexes to form palladium carboxylate complexes.

The rapid insertion of CO_2 into **1-Et** at room temperature enabled us to use NMR spectroscopy to measure the kinetics of the reaction. We performed kinetics experiments under pseudo-first order conditions with an excess of CO_2 and measured both the disappearance of **1-Et** and the appearance of **3-Et** (Fig. 8a). The reaction is first order in both **1-Et** and $[CO_2]$, so the overall rate law is $k_1[(^{tBu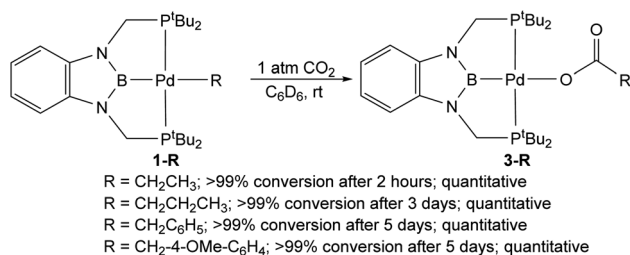}PBP)Pd(CH_2CH_3)][CO_2]$ (Fig. 8b and ESI†). We were able to obtain values of k_1 at different temperatures by dividing the k_{obs} values obtained from a plot of $\ln([(^{tBu}PBP)Pd(CH_2CH_3)])$ *versus* time by the concentration of CO_2 (Table 2 and ESI†). The most striking feature of our k_1 values is that at 40 °C, the rate constant for CO_2 insertion into **1-Et** is *more than double* the rate constant for insertion into **1-Me** that we measured previously.[13g] In the only other comparative study of the rates of CO_2 insertion into metal methyl and ethyl species, Darensbourg and co-workers observed that CO_2 insertion into $[RW(CO)_5]^-$ ($R = CH_3$ or CH_2CH_3) is 1.5 times faster for methyl than for ethyl, the opposite trend to our system.[8b] At this stage, given the paucity of other comparative studies on the rates of CO_2 insertion into different metal alkyls, it is unclear if either result is an outlier or the nature of the underlying factors that cause the variation in trends.

Using the values of k_1 at different temperatures we determined the activation parameters for CO_2 insertion into **1-Et** through Eyring analysis. The enthalpy of activation, $\Delta H^{\ddagger}$, is 11.3 ± 1.1 kcal mol^{-1}, the entropy of activation, $\Delta S^{\ddagger}$, is −29.0 ± 2.9 cal mol^{-1} K^{-1}, and $\Delta G^{\ddagger}_{298}$ is 20.0 ± 2.0 kcal mol^{-1} (see ESI†). All of these values are within error to those previously measured for **1-Me**,[13g] suggesting that the reactions proceed *via* similar pathways. The enthalpy for CO_2 insertion into **1-Et** is lower than that observed for insertion into palladium methyl complexes with pincer ligands that contain a lower *trans*-influence donor in the central position. For example, $\Delta H^{\ddagger}$ for CO_2 insertion into $(^{tBu}PCP)Pd(CH_3)$ ($^{tBu}PCP = 2,6\text{-}C_6H_3(CH_2P^tBu_2)_2$) is 17.4 ± 1.7 kcal mol^{-1}.[14b] This is consistent with the ^{tBu}PBP ligand destabilizing **1-Et** by weakening the Pd–C bond of the palladium

Table 2 Comparison of the rate constants for CO_2 insertion into $(^{tBu}PBP)Pd(alkyl)$ at various temperatures, solvents, and 1 atm of CO_2

Entry	Complex	Temperature (°C)	Solvent	k_1 (M^{-1} s^{-1} × 10^{-2})^a
1	**1-Et**	25	C_6D_6	1.2
2	**1-Et**	30	C_6D_6	2.1
3	**1-Et**	35	C_6D_6	2.9
4	**1-Et**	40	C_6D_6	3.4
5	**1-Et**	45	C_6D_6	4.7
6	**1-Me**	40	C_6D_6	1.3
7	**1-Me**	45	C_6D_6	2.3
8	**1-Bn**	30	Pyridine-d_5	0.48
9	**1-^{OMe}Bn**	30	Pyridine-d_5	0.43

^{a} These values are the average of two trials and the errors are ±10%.

ethyl ligand. The negative entropy of activation is similar to those observed in other systems for CO_2 insertion[13g,14b] and is in agreement with a rate-limiting transition state in which two molecules are combining to form one compound in the transition state.

The reaction of **1-^{n}Pr** with 1 atm of CO_2 in C_6D_6 at room temperature also cleanly generated the palladium carboxylate complex $(^{tBu}PBP)Pd\{OC(O)CH_2CH_2CH_3\}$ (**3-^{n}Pr**) (Fig. 6). Surprisingly, CO_2 insertion into **1-^{n}Pr** is significantly slower than the corresponding insertion reactions with **1-Me** and **1-Et**. In the case of **1-^{n}Pr**, the reaction required 3 days to reach completion at room temperature.[31] This slow rate of insertion precluded the measurement of a rate constant using our NMR method, but based on the reaction half-life of approximately 11 hours we estimate that insertion into **1-^{n}Pr** occurs approximately *one order of magnitude slower than* the rate of insertion into **1-Me**. Further, we were unable to heat the reaction of **1-^{n}Pr** with CO_2 to sufficiently speed up the reaction, as this resulted in decomposition of **1-^{n}Pr**. Overall, our results show that the simple change in alkyl group from **1-Me** to **1-Et** to **1-^{i}Pr** results in
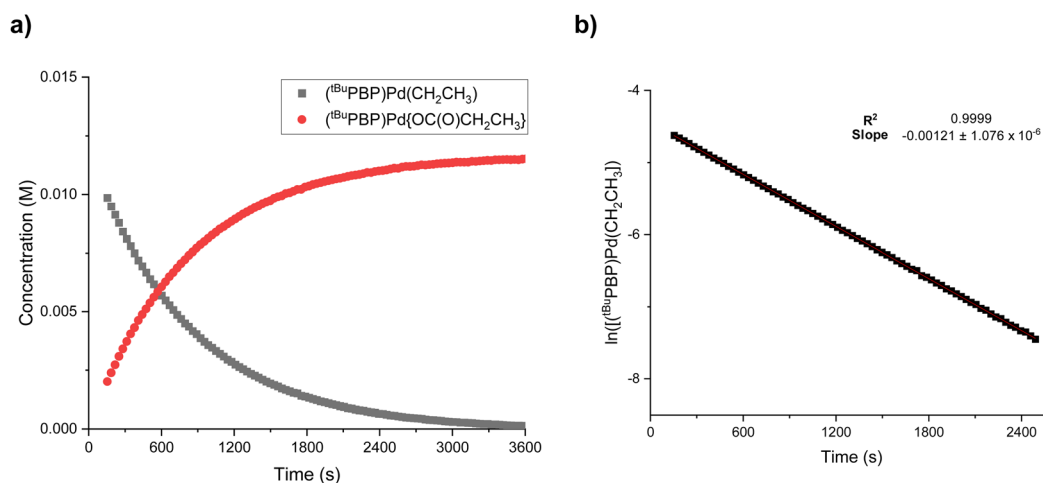
Fig. 8 Representative traces for the insertion of CO_2 into $(^{tBu}PBP)Pd(CH_2CH_3)$ (**1-Et**) at 30 °C in C_6D_6 with 1 atm of CO_2 showing (a) the concentrations of $(^{tBu}PBP)Pd(CH_2CH_3)$ (**1-Et**) and $(^{tBu}PBP)Pd\{OC(O)CH_2CH_3\}$ (**3-Et**) as a function of time and (b) the ln of the concentration of $(^{tBu}PBP)Pd(CH_2CH_3)$ (**1-Et**) as a function of time.

significant and non-intuitive changes in the rates of CO_2 insertion. This is potentially important in catalysis as it implies the rate of CO_2 insertion into palladium alkyl complexes (and potentially other metal alkyl complexes) will be heavily substrate dependent.

The reactions of the benzyl complexes **1-Bn** and **1-^{OMe}Bn** with 1 atm of CO_2 at room temperature formed the carboxylate complexes (^{tBu}PBP)Pd{OC(O)CH$_2$C$_6$H$_5$} (**3-Bn**) and (^{tBu}PBP)Pd {OC(O)CH$_2$-4-OMe-C$_6$H$_4$} (**3-^{OMe}Bn**), respectively (Fig. 6). These reactions were significantly slower than the corresponding insertion reactions with **1-Me**, **1-Et**, or even **1-^{n}Pr**. For example, in C_6D_6 at room temperature the reactions took approximately 5 days to reach completion. The slower rate of insertion into palladium benzyl complexes compared with palladium n-alkyl complexes is unsurprising as the benzylic carbon bound to palladium is expected to be a worse nucleophile due to the electron-withdrawing nature of the aromatic group, which makes it less energetically favorable to attack electrophilic CO_2. In order to measure the kinetics of insertion into **1-Bn** and **1-^{OMe}Bn** we needed to increase the rate of the reaction. Unfortunately, it is not possible to raise the temperature to promote CO_2 insertion into **1-Bn** in C_6D_6 as this leads to decomposition to form the palladium(0) complex, **2-Bn**, as well as the CO_2 inserted product. However, we have previously demonstrated that the rates of CO_2 insertion reactions can be increased by performing the reaction in solvents with a higher Dimroth–Reichardt $E_T(30)$ parameter,[13g,32] which is an empirical measure of the polarity of a solvent.[33,34] When CO_2 insertion reactions were performed in pyridine-d_5, the reactions with **1-Bn** and **1-^{OMe}Bn** were complete in approximately 5 hours at room temperature, with no evidence for the formation of palladium(0) complexes. This again highlights the dramatic effect of solvent on CO_2 insertion reactions.[13g,32,35] At 30 °C, the rate constants for CO_2 insertion into **1-Bn** and **1-^{OMe}Bn** in pyridine-d_5 were 0.0048 ± 0.0005 and 0.0043 ± 0.0004 M^{-1} s^{-1}, respectively. The fact that these values are the same within error indicates that the substitution on the phenyl ring surprisingly does not significantly affect the nucleophilicity of the carbon bound to palladium and means that in the catalytic carboxylation of benzylic substrates[36] the electronic effect of the substituents on the rate of CO_2 insertion is likely minimal. Unfortunately, we are unable to measure the rate constants for CO_2 insertion into **1-Me** or **1-Et** in pyridine-d_5 because the reaction occurs too fast to obtain an accurate rate constant using NMR spectroscopy. However, we estimate a minimum rate constant of 0.2 M^{-1} s^{-1}, which is significantly faster than for the benzyl compounds.

In contrast to our results with palladium alkyl complexes, no reaction was observed when **1-Ph** was treated with 1 atm of CO_2, even after prolonged heating at elevated temperature. Although at this stage it is unclear whether kinetic or thermodynamic factors are responsible for the lack of reactivity, our result is consistent with observations for other pincer supported Group 10 phenyl complexes, which also do not react with CO_2.[13b,e] Hence, although the PBP ligand promotes CO_2 insertion into palladium alkyl complexes, it does not facilitate insertion reactions into palladium aryl complexes.

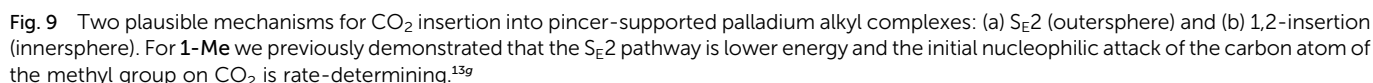## Computational studies of CO_2 insertion into palladium alkyl and aryl complexes

We performed DFT calculations (PBE0-D3BJ, IEFPCM) to further understand the mechanism of CO_2 insertion into **1-Me**, **1-Et**, **1-^{n}Pr**, **1-Bn**, and **1-^{OMe}Bn**. Previously, we have demonstrated that CO_2 insertion into **1-Me** follows an S_E2 (or outersphere) pathway (Fig. 9a),[13g] in which the first and rate-limiting step is nucleophilic attack of the carbon atom of the palladium methyl on the electrophilic carbon atom of CO_2 to form the C–C bond. Notably, there is no interaction between CO_2 and the palladium center at the transition state. The second step in CO_2 insertion into **1-Me** via an S_E2 pathway has a significantly lower barrier and involves the rearrangement of an carboxylate-palladium ion pair, bound through a C–H σ-bond, to the neutral Pd–O containing product.[13g] An alternative pathway involving 1,2-insertion (innersphere, Fig. 9b) in which both the Pd–O and C–C bonds are formed at the same transition state was calculated to be energetically unfavorable for **1-Me**.

Here, we calculated that for CO_2 insertion into **1-Et**, the barrier for the first step in the S_E2 pathway is 17.7 kcal mol^{-1} at 298 K (Fig. 10, Table 3).[37] This is in good agreement with the experimentally determined barrier of 20.0 ± 2.0 kcal mol^{-1} (vide supra). The barrier for the innersphere 1,2-insertion pathway is calculated to be 26.0 kcal mol^{-1}, unambiguously indicating that the S_E2 pathway is preferred. A surprising feature of **1-Et** is that it does not undergo facile β-hydride elimination. We calculated that the barrier for β-hydride elimination is relatively high (32.3 kcal mol^{-1}), consistent with the stability of the complex towards β-hydride elimination. β-Hydride elimination is presumably disfavored because of the rigidity of the pincer ligand, which makes it energetically difficult for the complex to distort to form the syn co-planar arrangement of the palladium, C_α, C_β, and H required for β-hydride elimination.

DFT calculations predict that the barriers for CO_2 insertion into **1-Me** and **1-^{n}Pr** are 19.4 kcal mol^{-1} and 21.8 kcal mol^{-1} (Table 3), respectively, which means that the calculations are in line with the experimental trends in rate (**1-Et** > **1-Me** > **1-^{n}Pr**).[38] The rate-determining transition states for CO_2 insertion into **1-Me**, **1-Et**, and **1-^{n}Pr** are analogous (the first step in the S_E2 mechanism), so the differences in rate are not related to a change in mechanism. Instead, we propose that the difference in rates is due primarily to steric factors, which affect the relative stability of both the reactant complexes and the transition states. **1-Et** and **1-^{n}Pr** are likely slightly destabilized relative to **1-Me** because of steric interactions between the ethyl or propyl ligand and the tert-butyl substituents of the ^{tBu}PBP ligand. This is reflected by the increased thermodynamic favorability of CO_2 insertion into **1-Et** and **1-^{n}Pr** compared to **1-Me** ($\Delta G° = -27.5$ and -26.2 kcal mol^{-1}, respectively, versus -22.9 kcal mol^{-1}). Presumably, in the carboxylate complexes, the steric pressure is relieved because of the absence of hydrogens on the oxygen bound to palladium.

The steric properties of **1-Me**, **1-Et**, and **1-^{n}Pr** were quantitatively evaluated by calculating the percent buried volume (% V_{Bur}) of these complexes based on their crystal structures using the Salerno molecular buried volume program (SambVca 2.1)

Fig. 9 Two plausible mechanisms for CO_2 insertion into pincer-supported palladium alkyl complexes: (a) S_E2 (outersphere) and (b) 1,2-insertion (innersphere). For **1-Me** we previously demonstrated that the S_E2 pathway is lower energy and the initial nucleophilic attack of the carbon atom of the methyl group on CO_2 is rate-determining.[13g]

(Fig. 11).[39] Although there is only a small difference in $\%V_{Bur}$ between the three complexes (86.9% for **1-Me**, 87.7% for **1-Et**, and 88.2% for **1-^{n}Pr**) the absolute magnitude of these numbers indicates the high degree of steric crowding around the palladium centers and suggests that small changes could have a significant impact on the rate of CO_2 insertion. Our proposal is that **1-Et** is sufficiently sterically crowded to destabilize the

ethyl ligand, but still open enough for CO_2 to easily approach the ethyl group. This increases the rate of insertion in comparison to **1-Me**. In contrast, even though **1-^{n}Pr** is sufficiently sterically crowded to destabilize the n-propyl ligand, the complex is so congested that it is unfavorable for CO_2 to approach, which increases the barrier for insertion. Consistent with this proposal, the computed barrier for CO_2 insertion into

Fig. 10 Relative free energies of CO_2 insertion into **1-Et** via an S_E2 (outersphere) and 1,2-addition (innersphere) pathway, as well as the energy for β-hydride elimination. In the S_E2 pathway, we were unable to find the intermediate and barrier for the second rearrangement step to form the palladium carboxylate product, as the rearrangement occurs spontaneously during geometry optimization. However, this process has previously been demonstrated to be low energy in related systems.[13g]

Table 3 Calculated barriers for CO_2 insertion into $(^RPBP)Pd(alkyl)$ complexes

Complex	$\Delta G^{\ddagger}$ (kcal mol^{-1})
$(^{tBu}PBP)Pd(CH_3)$ (**1-Me**)	19.4
$(^{tBu}PBP)Pd(CH_2CH_3)$ (**1-Et**)	17.7
$(^{tBu}PBP)Pd(CH_2CH_2CH_3)$ (**1-^{n}Pr**)	21.8
$(^{tBu}PBP)Pd\{CH(CH_3)_2\}$ (**1-^{i}Pr**)	28.2
$(^{tBu}PBP)Pd(CH_2C_6H_5)$ (**1-Bn**)	20.3
$(^{tBu}PBP)Pd(CH_2\text{-}4\text{-}OMeC_6H_4)$ (**1-^{OMe}Bn**)	20.5
$(^{tBu}PBP)Pd(CH_2\text{-}4\text{-}CF_3C_6H_4)$ (**1-^{CF3}Bn**)	20.6
$(^{tBu}PBP)Pd(C_6H_5)$ (**1-Ph**)	34.6[a]
$(^{iPr}PBP)Pd(CH_3)$	16.8[a]
$(^{iPr}PBP)Pd(CH_2CH_3)$	18.7
$(^{iPr}PBP)Pd(CH_2CH_2CH_3)$	20.3
$(^{Me}PBP)Pd(CH_3)$	17.5[a]
$(^{Me}PBP)Pd(CH_2CH_3)$	17.3[a]
$(^{Me}PBP)Pd(CH_2CH_2CH_3)$	17.5[a]

[a] The lowest energy pathway for CO_2 insertion is the 1,2-insertion (or innersphere) mechanism rather than the S_E2 (or outersphere) mechanism.

the even more sterically congested $(^{tBu}PBP)Pd\{CH(CH_3)_2\}$ (**1-^{i}Pr**) increases to 28.2 kcal mol^{-1} (Table 3). Finally, the trajectory of electrophilic attack of CO_2 is quite different for **1-Me** compared to **1-Et** and **1-^{n}Pr**. In **1-Me** the CO_2 is nearly orthogonal to the palladium methyl bond, whereas in **1-Et** and **1-^{n}Pr** is it essentially co-planar (Fig. 12). In **1-Et** and **1-Pr** this geometry leads to close contacts between three C–H bonds and the incipient carboxylate group, which may help stabilize the emerging charge on the carboxylate group. We were unable to locate a similar TS geometry for insertion into **1-Me**, and in the calculated TS there are only interactions between two C–H bonds and the incipient carboxylate group. In the case of **1-Pr**, destabilization due to steric strain is likely a larger force than stabilization due to an extra non-covalent interaction and therefore the overall barrier is higher.

To further probe the role of steric factors on the rates of CO_2 insertion, we performed calculations on the smaller model complexes $(^RPBP)Pd(alkyl)$ (R = Me or ^{i}Pr; alkyl = CH_3, CH_2CH_3, or $CH_2CH_2CH_3$). Interestingly, in the case of ^{Me}PBP, DFT predicts that the preferred CO_2 insertion pathway changes from

S_E2 to 1,2-insertion for all tested alkyls (see ESI†), suggesting that the size of the ligand is crucial in determining the reaction pathway. We propose that complexes with a smaller steric profile are more likely to react *via* a 1,2-insertion pathway compared with complexes that are more congested, because in this case it is easier for CO_2 to interact with the metal center. Further, in the case of ^{Me}PBP supported complexes, the calculated rates of insertion are the same for the methyl, ethyl, and n-propyl species, suggesting that the nature of the alkyl group is less important for systems that react through a 1,2-insertion pathway. This is unsurprising, as in the 1,2-insertion pathway the metal center is directly involved, which likely lessens the impact of the alkyl group. For the ^{iPr}PBP supported palladium complexes, 1,2-insertion is preferred for $(^{iPr}PBP)Pd(CH_3)$, whereas the S_E2 pathway is preferred for the ethyl and propyl complexes, with the later showing higher barriers than $(^{iPr}PBP)Pd(CH_3)$. The barrier for insertion into $(^{iPr}PBP)Pd(CH_2CH_3)$ is lower than for $(^{iPr}PBP)Pd(CH_2CH_2CH_3)$, indicating that there is a steric effect with the ^{iPr}PBP pincer ligand. The computed results with the smaller ancillary ligands suggest that the observation that CO_2 insertion is faster for **1-Et** than for **1-Me** or **1-^{n}Pr** is unlikely to be general to all systems. The ^{tBu}PBP ligand creates a sufficiently crowded environment where a minor change in the sterics results in non-intuitive changes in rate, whereas for other supporting ligands this will not be the case, as evidenced by our calculated results with ^{iPr}PBP and ^{Me}PBP.

We next investigated the barriers for CO_2 insertion into the palladium benzyl complexes **1-Bn**, **1-^{OMe}Bn**, as well as the hypothetical complex $(^{tBu}PBP)Pd(CH_2\text{-}4\text{-}CF_3\text{-}C_6H_4)$ (**1-^{CF3}Bn**) (Table 3). The calculated barrier for CO_2 insertion into **1-Bn** (20.3 kcal mol^{-1}) is higher than for **1-Me** and **1-Et**, in agreement with our experimental observations. In contrast, we computationally predict that insertion into **1-^{n}Pr** is more challenging than insertion into **1-Bn**, which contradicts our experimental results, but likely reflects some computational error. When calculations were performed with other functionals (see ESI†), there were cases where the barrier for insertion into **1-Bn** was higher than for **1-^{n}Pr**, indicating that different DFT functionals provide slighty different TS structures. The lowest energy pathway for insertion into **1-Bn** involves an S_E2 mechanism and the geometric parameters at the transition state for insertion are similar to those observed for **1-Me**, **1-Et**, and **1-^{n}Pr**. Previous
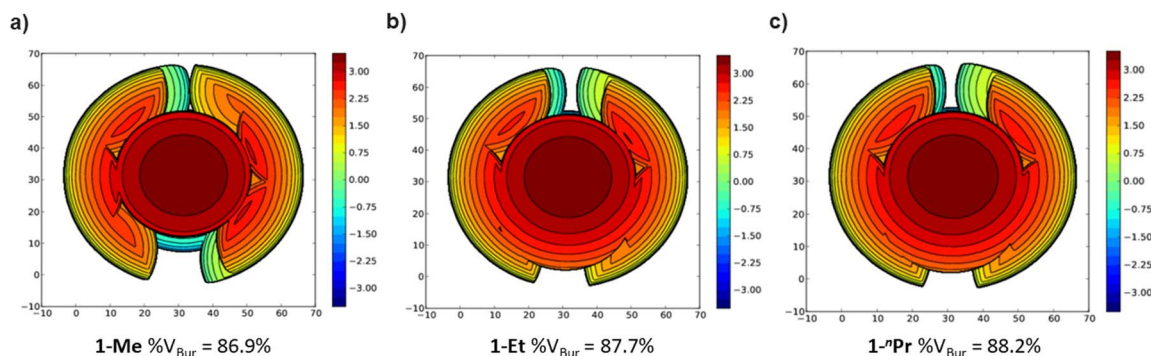

Fig. 11 Topographic steric maps of (a) **1-Me**, (b) **1-Et**, and (c) **1-^{n}Pr** as viewed down the C–Pd bond towards the plane defined by P–Pd–P.[39]
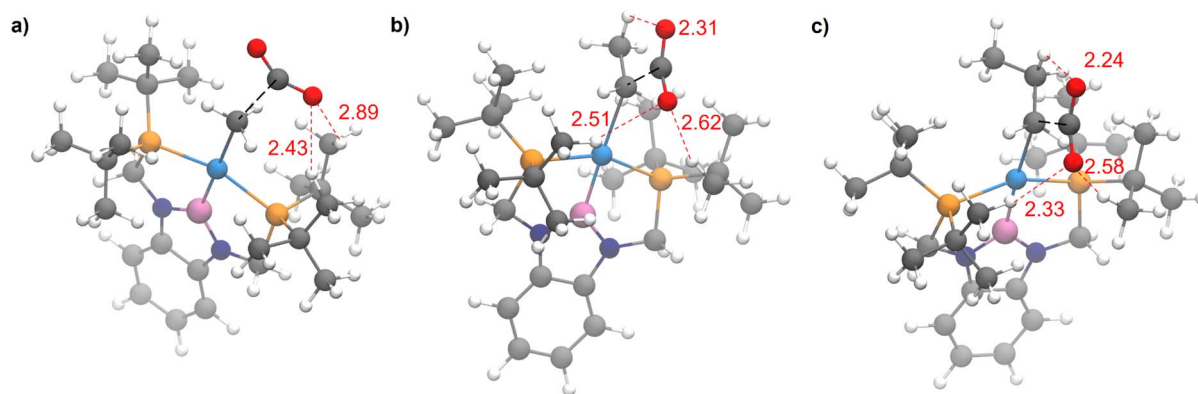
Fig. 12 Rate determining transition states for CO_2 insertion into (a) **1-Me**, (b) **1-Et**, and (c) **1-^{n}Pr**. Close contacts between ligand C–H bonds and the incipient carboxylate group are highlighted in red. The bond forming atoms are connected by a dotted black line.

calculations on CO_2 insertion into palladium benzyl species have also invoked an S_E2 pathway.[40] Calculations on CO_2 insertion into **1-^{OMe}Bn** or **1-^{CF_3}Bn** indicate that the barriers for insertion into these species are approximately the same as for the unsubstituted palladium benzyl species. This is unexpected as it suggests that the impact of the para-substituent on the nucleophilicity of the benzylic carbon is negligible even though this substituent should impact the energy of the π^*-orbital which stabilizes or destabilizes the carbon. Nevertheless, our calculations are in agreement with the experimental rate constants of **1-Bn** and **1-^{OMe}Bn** being within error (*vide supra*).

In contrast to the facile insertion of CO_2 into palladium alkyl complexes supported by ^{tBu}PBP ligands, we did not observe CO_2 insertion into **1-Ph**. To understand this reactivity, we calculated the kinetic and thermodynamic parameters associated with CO_2 insertion into **1-Ph**. Although the reaction is considerably thermodynamically downhill (by −19.2 kcal mol^{-1}), the kinetic barrier is 34.6 kcal mol^{-1}, which explains why no reaction is observed experimentally. Consistent with our previous results for CO_2 insertion into palladium–C(sp^2) bonds,[40] the transition state is classified as innersphere, with a Pd–C$_{CO_2}$ interaction of 3.03 Å. To understand the influence of the ^{tBu}PBP ligand on CO_2 insertion into **1-Ph**, we calculated the energy of the transition state for CO_2 insertion into (^{tBu}PCP)Pd(C$_6$H$_5$) (^{tBu}PCP = 2,6-C$_6$-H$_3$(CH$_2$P^{t}Bu$_2$)$_2$), which features a pincer ligand with a lower *trans*-influence donor opposite the phenyl group. In this case, the activation energy associated with an innersphere transition state is 46.3 kcal mol^{-1}, indicating that influence of the ^{tBu}PBP ligand is significant. However, in order for CO_2 insertion to become kinetically viable experimentally, a different approach needs to be adopted than introducing a stronger *trans*-influence ligand opposite the phenyl ligand, as the ^{tBu}PBP ligand is one of the strongest *trans*-influence ligands available and it does not lower the activation energy for CO_2 insertion enough for the reaction to proceed under mild conditions.

Conclusions

In this work, we prepared and crystallographically characterized an unusual series of ^{tBu}PBP supported palladium alkyl and aryl

complexes including species with ethyl, n-propyl, benzyl, and phenyl ligands. In contrast, ^{tBu}PBP supported palladium complexes with n-butyl, iso-propyl, and *tert*-butyl ligands were either unstable or could not be observed. The rates of decomposition of the alkyl complexes are related to the steric bulk of the alkyl ligand with a putative *tert*-butyl complex decomposing faster than the ethyl species. The palladium alkyl complexes decompose *via* two different routes. The least and most sterically bulky complexes containing ethyl or *tert*-butyl ligands decompose *via* β-hydride elimination. In contrast, complexes containing n-butyl and iso-propyl ligands are stable towards β-hydride elimination and along with benzyl complexes decompose *via* an uncommon reductive coupling reaction, which involves the formation of a new C–B bond and either well-defined palladium(0) dimers or palladium black. Attempts to synthesize a ^{tBu}PBP supported palladium hydride were unsuccessful because a similar reductive coupling occurred to generate a dimeric palladium(0) complex with two new H–B bonds. The observation of decomposition *via* reductive coupling across a series of complexes confirms that this is a general reaction for ^{R}PBP supported complexes.

^{tBu}PBP ligated palladium complexes with ethyl, n-propyl, and benzyl ligands all cleanly insert CO_2 to form the corresponding carboxylate complexes, allowing for a rare study of the rates of CO_2 insertion across an analogous series of metal alkyl complexes. Kinetic studies demonstrate that the rate of CO_2 insertion into **1-Et** is more than double the rate for insertion into **1-Me**, which in turn is ten times faster than the rate of insertion into **1-^{n}Pr**. CO_2 insertion into ^{tBu}PBP supported palladium benzyl complexes is much slower than insertion into n-alkyl complexes, likely because the carbon atom of the benzyl group is less nucleophilic. DFT calculations indicate that insertion reactions into **1-Me**, **1-Et**, **1-^{n}Pr**, and **1-Bn** proceed *via* an outersphere S_E2 pathway and steric factors are responsible for the observed differences in rate between the n-alkyl complexes. They also suggest that the counterintuitive trends in the rates of CO_2 insertion observed in the present work will not occur for all metal alkyl systems but are related to the specific steric factors present in this group of complexes. Although the strong *trans*-influence of the boryl ligand in ^{tBu}PBP

promotes CO_2 insertion into palladium alkyl complexes, no reaction is observed between **1-Ph** and CO_2. Overall, our results highlight how the rates of CO_2 vary across an analogous series of palladium alkyl and aryl complexes and DFT calculations provide explanations for the observed trends. This information will be valuable for the development of catalytic reactions that involve CO_2 insertion into metal alkyl bonds as an elementary step.

Data availability

Crystallographic data has been deposited at the CCDC with numbers 2243696–2243703 and 2264960. NMR spectra and the coordinates and energies of DFT optimized geometries are provided as part of the ESI.†

Author contributions

APD and NH conceptualized the project. APD performed experimental investigations and SG performed computational investigations. NH supervised experimental studies and KHH supervised computational studies. All authors were involved in writing the manuscript.

Conflicts of interest

The authors declare no competing financial interests.

Acknowledgements

References

1 (a) E. A. Quadrelli, G. Centi, J.-L. Duplan and S. Perathoner, Carbon Dioxide Recycling: Emerging Large-Scale Technologies with Industrial Potential, *ChemSusChem*, 2011, **4**, 1194–1215; (b) A. M. Appel, J. E. Bercaw, A. B. Bocarsly, H. Dobbek, D. L. DuBois, M. Dupuis, J. G. Ferry, E. Fujita, R. Hille, P. J. A. Kenis, C. A. Kerfeld, R. H. Morris, C. H. F. Peden, A. R. Portis, S. W. Ragsdale, T. B. Rauchfuss, J. N. H. Reek, L. C. Seefeldt, R. K. Thauer and G. L. Waldrop, Frontiers, Opportunities, and Challenges in Biochemical and Chemical Catalysis of CO_2 Fixation, *Chem. Rev.*, 2013, **113**, 6621–6658; (c) W.-H. Wang, Y. Himeda, J. T. Muckerman, G. F. Manbeck and E. Fujita, CO_2 Hydrogenation to Formate and Methanol as an Alternative to Photo- and Electrochemical CO_2 Reduction, *Chem. Rev.*, 2015, **115**, 12936–12973; (d) W. H. Bernskoetter and N. Hazari, Reversible Hydrogenation of Carbon Dioxide to Formic Acid and Methanol: Lewis Acid

Enhancement of Base Metal Catalysts, *Acc. Chem. Res.*, 2017, **50**, 1049–1058; (e) J. Artz, T. E. Müller, K. Thenert, J. Kleinekorte, R. Meys, A. Sternberg, A. Bardow and W. Leitner, Sustainable Conversion of Carbon Dioxide: An Integrated Review of Catalysis and Life Cycle Assessment, *Chem. Rev.*, 2018, **118**, 434–504; (f) N. Onishi, G. Laurenczy, M. Beller and Y. Himeda, Recent Progress for Reversible Homogeneous Catalytic Hydrogen Storage in Formic Acid and in Methanol, *Coord. Chem. Rev.*, 2018, **373**, 317–332; (g) M. D. Burkart, N. Hazari, C. L. Tway and E. L. Zeitler, Opportunities and Challenges for Catalysis in Carbon Dioxide Utilization, *ACS Catal.*, 2019, **9**, 7937–7956; (h) C. Hepburn, E. Adlen, J. Beddington, E. A. Carter, S. Fuss, N. Mac Dowell, J. C. Minx, P. Smith and C. K. Williams, The Technological and Economic Prospects for CO_2 Utilization and Removal, *Nature*, 2019, **575**, 87–97; (i) Z. Zhang, S.-Y. Pan, H. Li, J. Cai, A. G. Olabi, E. J. Anthony and V. Manovic, Recent Advances in Carbon Dioxide Utilization, *Renewable Sustainable Energy Rev.*, 2020, **125**, 109799; (j) W. Gao, S. Liang, R. Wang, Q. Jiang, Y. Zhang, Q. Zheng, B. Xie, C. Y. Toe, X. Zhu, J. Wang, L. Huang, Y. Gao, Z. Wang, C. Jo, Q. Wang, L. Wang, Y. Liu, B. Louis, J. Scott, A.-C. Roger, R. Amal, H. He and S.-E. Park, Industrial Carbon Dioxide Capture and Utilization: State of the Art and Future Challenges, *Chem. Soc. Rev.*, 2020, **49**, 8584–8686; (k) S. Overa, T. G. Feric, A.-H. A. Park and F. Jiao, Tandem and Hybrid Processes for Carbon Dioxide Utilization, *Joule*, 2021, **5**, 8–13; (l) T. Singh, S. Jalwal and S. Chakraborty, Homogeneous First-row Transition-metal-catalyzed Carbon Dioxide Hydrogenation to Formic Acid/Formate, and Methanol, *Asian J. Org. Chem.*, 2022, **11**, e202200330; (m) C. Das, J. Grover, Tannu, A. Das, D. Maiti, A. Dutta and G. K. Lahiri, Recent Developments in First-Row Transition Metal Complex-Catalyzed CO_2 Hydrogenation, *Dalton Trans.*, 2022, **51**, 8160–8168; (n) N. Onishi and Y. Himeda, Homogeneous Catalysts for CO_2 Hydrogenation to Methanol and Methanol Dehydrogenation to Hydrogen Generation, *Coord. Chem. Rev.*, 2022, **472**, 214767.

2 National Academies of Sciences, and Engineering, and Medicine, *Gaseous Carbon Waste Streams Utilization: Status and Research Needs*, The National Academies Press, Washington DC, 2019.

3 N. Hazari and J. E. Heimann, Carbon Dioxide Insertion into Group 9 and 10 Metal-Element σ-Bonds, *Inorg. Chem.*, 2017, **56**, 13655–13678.

4 (a) M. Börjesson, T. Moragas, D. Gallego and R. Martin, Metal-Catalyzed Carboxylation of Organic (Pseudo)halides with CO_2, *ACS Catal.*, 2016, **6**, 6739–6749; (b) A. Tortajada, F. Juliá-Hernández, M. Börjesson, T. Moragas and R. Martin, Transition-Metal-Catalyzed Carboxylation Reactions with Carbon Dioxide, *Angew. Chem., Int. Ed.*, 2018, **57**, 15948–15982.

5 For an example of CO_2 insertion into a Sc-alkyl bond see: F. A. LeBlanc, A. Berkefeld, W. E. Piers and M. Parvez, Reactivity of Scandium β-Diketiminate Alkyl Complexes with Carbon Dioxide, *Organometallics*, 2012, **31**, 810–818.

6 For an example of CO_2 insertion into a Zr-alkyl bond see: K.-C. Lau, B. J. Petro, S. Bontemps and R. F. Jordan, Comparative Reactivity of Zr– and Pd–Alkyl Complexes with Carbon Dioxide, *Organometallics*, 2013, **32**, 6895–6898.

7 For an example of CO_2 insertion into a Cr-alkyl bond see: D. J. Darensbourg and A. Rokicki, Reduction of Carbon Dioxide and Carbonyl Sulfide by Anionic Group VIB Metal Hydrides and Alkyls. Carbon-Hydrogen and Carbon-Carbon Bond Formation Processes and the Structure of [PNP] [Cr(CO)$_5$SC(O)H], *J. Am. Chem. Soc.*, 1982, **104**, 349–350.

8 For examples of CO_2 insertion into W-alkyl bonds see:(a) D. J. Darensbourg and R. Kudaroski, Metal-Induced Transformations of Carbon Dioxide. Carbon-Carbon Bond-Forming Processes Involving Anionic Group VIB Metal Derivatives, and the X-ray structure of [PNP][cis-MeW(CO)$_4$PMe$_3$], *J. Am. Chem. Soc.*, 1984, **106**, 3672–3673; (b) D. J. Darensbourg, R. K. Hanckel, C. G. Bauch, M. Pala, D. Simmons and J. N. White, A Kinetic Investigation of Carbon Dioxide Insertion Processes Involving Anionic Tungsten-Alkyl and -Aryl Derivatives: Effects of Carbon Dioxide Pressure, Counterions, and Ancillary Ligands. Comparisons with Migratory Carbon Monoxide Insertion Processes, *J. Am. Chem. Soc.*, 1985, **107**, 7463–7473; (c) D. J. Darensbourg and M. Pala, Cation-Anion Interaction in the [Na-kryptofix-221][W(CO)$_5$O$_2$CH] Derivative and its Relevance in Carbon Dioxide Reduction Processes, *J. Am. Chem. Soc.*, 1985, **107**, 5687–5693; (d) D. J. Darensbourg and G. Grotsch, Stereochemical Studies of the Carbon Dioxide Insertion Reactions into the Tungsten-Alkyl Bond, *J. Am. Chem. Soc.*, 1985, **107**, 7473–7476.

9 For examples of CO_2 insertion into Fe-alkyl bonds see:(a) S. Ittel, C. Tolman, A. English and J. Jesson, The Chemistry of 2-Naphthyl bis[bis(dimethylphosphino)ethane] Hydride Complexes of Iron, Ruthenium, and Osmium. 2. Cleavage of sp and sp^3 Carbon-Hydrogen, Carbon-Oxygen, and Carbon-Halogen bonds. Coupling of Carbon Dioxide and Acetonitrile, *J. Am. Chem. Soc.*, 1978, **100**, 7577–7585; (b) I. M. Arafa, K. Shin and H. M. Goff, Carbon Monoxide and Carbon Dioxide Carbon-Metal Bond Insertion Chemistry of Alkyliron(III) Porphyrin Complexes, *J. Am. Chem. Soc.*, 1988, **110**, 5228–5229; (c) O. R. Allen, S. J. Dalgarno, L. D. Field, P. Jensen, A. J. Turnbull and A. C. Willis, Addition of CO_2 to Alkyl Iron complexes, Fe(PP)$_2$Me$_2$, *Organometallics*, 2008, **27**, 2092–2098; (d) K.-C. Lau and R. F. Jordan, Reactivity of (Pyridine-Diimine) Fe Alkyl Complexes with Carbon Dioxide, *Organometallics*, 2016, **35**, 3658–3666.

10 For examples of CO_2 insertion into Ru-alkyl bonds see:(a) J. F. Hartwig, R. G. Bergman and R. A. Andersen, Insertion Reactions of Carbon Monoxide and Carbon Dioxide with Ruthenium Benzyl, Arylamido, and Aryloxide complexes: A Comparison of the Reactivity of Ruthenium-Carbon, Ruthenium-Nitrogen, and Ruthenium-Oxygen Bonds, *J. Am. Chem. Soc.*, 1991, **113**, 6499–6508; (b) O. R. Allen, S. J. Dalgarno, L. D. Field, P. Jensen and A. C. Willis, Insertion of CO_2 into the Ru–C Bonds of cis-and trans-Ru(dmpe)$_2$Me$_2$ (dmpe = Me$_2$PCH$_2$CH$_2$PMe$_2$), *Organometallics*, 2009, **28**, 2385–2390.

11 For examples of CO_2 insertion into Rh-alkyl bonds see:(a) D. J. Darensbourg, G. Groetsch, P. Wiegreffe and A. L. Rheingold, Insertion Reactions of Carbon Dioxide with Square-Planar Rhodium Alkyl and Aryl Complexes, *Inorg. Chem.*, 1987, **26**, 3827–3830; (b) T. G. Ostapowicz, M. Hölscher and W. Leitner, CO_2 Insertion into Metal–Carbon Bonds: A Computational Study of RhI Pincer Complexes, *Chem.–Eur. J.*, 2011, **17**, 10329–10338; (c) T. Suga, T. Saitou, J. Takaya and N. Iwasawa, Mechanistic Study of the Rhodium-Catalyzed Carboxylation of Simple Aromatic Compounds with Carbon Dioxide, *Chem. Sci.*, 2017, **8**, 1454–1462; (d) L. Pavlovic, J. Vaitla, A. Bayer and K. H. Hopmann, Rhodium-Catalyzed Hydrocarboxylation: Mechanistic Analysis Reveals Unusual Transition State for Carbon–Carbon Bond Formation, *Organometallics*, 2018, **37**, 941–948.

12 For examples of CO_2 insertion into Cu-alkyl bonds see:(a) T. Ikariya and A. Yamamoto, Preparation and Properties of Ligand-Free Methylcopper and of Copper Alkyls Coordinated with 2,2′-Bipyridyl and Tricyclohexylphosphine, *J. Organomet. Chem.*, 1974, **72**, 145–151; (b) S. Sakaki and K. Ohkubo, Ab initio MO Study of Carbon Dioxide Insertion into a Methyl-Copper(I) Bond. Critical Difference from CO_2 Insertion into a Hydrogen-Copper(I) Bond, *Organometallics*, 1989, **8**, 2970–2973; (c) N. P. Mankad, T. G. Gray, D. S. Laitar and J. P. Sadighi, Synthesis, Structure, and CO_2 Reactivity of a Two-Coordinate (Carbene)copper(I) Methyl Complex, *Organometallics*, 2004, **23**, 1191–1193.

13 For examples of CO_2 insertion into Ni-alkyl bonds see:(a) T. J. Schmeier, N. Hazari, C. D. Incarvito and J. R. Raskatov, Exploring the Reactions of CO_2 with PCP Supported Nickel Complexes, *Chem. Commun.*, 2011, **47**, 1824–1826; (b) K. J. Jonasson and O. F. Wendt, Synthesis and Characterization of a Family of POCOP Pincer Complexes with Nickel: Reactivity Towards CO_2 and Phenylacetylene, *Chem.–Eur. J.*, 2014, **20**, 11894–11902; (c) A. H. Mousa, J. Bendix and O. F. Wendt, Synthesis, Characterization, and Reactivity of PCN Pincer Nickel Complexes, *Organometallics*, 2018, **37**, 2581–2593; (d) A. H. Mousa, A. V. Polukeev, J. Hansson and O. F. Wendt, Carboxylation of the Ni–Me Bond in an Electron-Rich Unsymmetrical PCN Pincer Nickel Complex, *Organometallics*, 2020, **39**, 1553–1560; (e) J. B. Diccianni, C. T. Hu and T. Diao, Insertion of CO_2 Mediated by a (Xantphos)NiI–Alkyl Species, *Angew. Chem., Int. Ed.*, 2019, **58**, 13865–13868; (f) R. J. Somerville, C. Odena, M. F. Obst, N. Hazari, K. H. Hopmann and R. Martin, Ni(I)–Alkyl Complexes Bearing Phenanthroline Ligands: Experimental Evidence for CO_2 Insertion at Ni(I) Centers, *J. Am. Chem. Soc.*, 2020, **142**, 10936–10941; (g) A. P. Deziel, M. R. Espinosa, L. Pavlovic, D. J. Charboneau, N. Hazari, K. H. Hopmann and B. Q. Mercado, Ligand and Solvent Effects on CO_2 Insertion into Group 10 Metal Alkyl Bonds, *Chem. Sci.*, 2022, **13**, 2391–2404.

14 For examples of CO_2 insertion into Pd-alkyl bonds see references [6], 13f and:(a) R. Johansson, M. Jarenmark and

O. F. Wendt, Insertion of Carbon Dioxide into (PCP)Pd^{II}-Me Bonds, *Organometallics*, 2005, **24**, 4500–4502; (*b*) M. T. Johnson, R. Johansson, M. V. Kondrashov, G. Steyl, M. S. G. Ahlquist, A. Roodt and O. F. Wendt, Mechanisms of the CO$_2$ Insertion into (PCP) Palladium Allyl and Methyl σ-Bonds. A Kinetic and Computational Study, *Organometallics*, 2010, **29**, 3521–3529.

15 H.-W. Suh, L. M. Guard and N. Hazari, A Mechanistic Study of Allene Carboxylation with CO$_2$ Resulting in the Development of a Pd(II) Pincer Complex for the Catalytic Hydroboration of CO$_2$, *Chem. Sci.*, 2014, **5**, 3859–3872.

16 The change from an organolithium reagent in the synthesis of (*t*BuPBP)Pd(CH2CH3) to a Grignard reagent for the preparation of (*t*BuPBP)Pd(CH2CH2CH3) is because EtLi is commercially available but *n*PrLi is not. In contrast, *n*PrMgCl is commercially available.

17 (*a*) J. Takaya and N. Iwasawa, Synthesis, Structure, and Reactivity of a Mononuclear η^2-(Ge–H)palladium(0) Complex Bearing a PGeP-Pincer-Type Germyl Ligand: Reactivity Differences between Silicon and Germanium, *Eur. J. Inorg. Chem.*, 2018, **2018**, 5012–5018; (*b*) M.-H. Huang, W.-Y. Lee, X.-R. Zou, C.-C. Lee, S.-B. Hong and L.-C. Liang, Amido PNP Pincer Complexes of Palladium(II) and Platinum(II): Synthesis, Structure, and Reactivity, *Appl. Organomet. Chem.*, 2021, **35**, e6128.

18 D. L. Reger, D. G. Garza and L. Lebioda, Synthesis of Extremely Stable Alkylpalladium Complexes of the type (Me$_2$NCS$_2$)Pd(PEt$_3$)(alkyl). Crystal and Molecular Structures of the Isomers [cyclic](CH$_2$CH$_2$CH$_2$CH$_2$NCS$_2$)Pd(PEt$_3$)(n-propyl) and [cyclic](CH$_2$CH$_2$CH$_2$CH$_2$NCS$_2$)Pd(PEt$_3$)(isopropyl), *Organometallics*, 1991, **10**, 902–906.

19 Y. Ding, Q.-Q. Ma, J. Kang, J. Zhang, S. Li and X. Chen, Palladium(II) Complexes Supported by PBP and POCOP Pincer Ligands: A Comparison of their Structure, Properties and Catalytic Activity, *Dalton Trans.*, 2019, **48**, 17633–17643.

20 (*a*) K. Osakada, Y. Ozawa and A. Yamamoto, Preparation and Properties of Ethylpalladium Thiolate Complexes. Reaction with Organic Halides Leading to C–S Bond Formation; Crystal Structure of Trans-[PdEt(Br)(PMe$_3$)$_2$], *J. Chem. Soc., Dalton Trans.*, 1991, 759–764; (*b*) K. Osakada, Y. Ozawa and A. Yamamoto, Molecular Structure and Carbonylation of Ethyl(benzenethiolato)-palladium(II) Complex, trans-PdEt(SPh)(PMe$_3$)$_2$, *Bull. Chem. Soc. Jpn.*, 1991, **6**, 2002–2004; (*c*) A. J. Canty, H. Jin, A. S. Roberts, B. W. Skelton, P. R. Traill and A. H. White, Synthesis and Characterization of Ambient Temperature Stable Organopalladium(IV) Complexes, Including Aryl-, η^1-Allyl-, Ethylpalladium(IV), and Pallada(IV)cyclopentane Complexes. Structures of the Poly(pyrazol-1-yl)borate Complexes PdMe$_3${(pz)$_3$BH} and PdMe$_3${(pz)$_4$B} and Three Polymorphs of PdMe$_2$Et{(pz)$_3$BH, *Organometallics*, 1995, **14**, 199–206; (*d*) R. A. Stockland Jr, G. K. Anderson and N. P. Rath, Hydride-Bridged Dipalladium Complexes Containing Diphosphine Ligands, *Inorg. Chim. Acta*, 1997, **259**, 173–178; (*e*) R. A. Stockland Jr, G. K. Anderson and N. P. Rath, Synthesis and Structures of Hydride-Bridged

Palladium A-Frame Complexes, *Inorg. Chim. Acta*, 2000, **300**, 395–405.

21 (*a*) Z. Csok, O. Vechorkin, S. B. Harkins, R. Scopelliti and X. Hu, Nickel Complexes of a Pincer NN2 Ligand: Multiple Carbon–Chloride Activation of CH$_2$Cl$_2$ and CHCl$_3$ Leads to Selective Carbon–Carbon Bond Formation, *J. Am. Chem. Soc.*, 2008, **130**, 8156–8157; (*b*) L.-C. Liang, W.-Y. Lee, Y.-T. Hung, Y.-C. Hsiao, L.-C. Cheng and W.-C. Chen, Nickel Complexes Incorporating an Amido Phosphine Chelate with a endant Amine Arm: Synthesis, Structure, and Catalytic Kumada Coupling, *Dalton Trans.*, 2012, **41**, 1381–1388; (*c*) C. Yoo, S. Oh, J. Kim and Y. Lee, Transmethylation of a Four-Coordinate Nickel(I) Monocarbonyl Species with Methyl Iodide, *Chem. Sci.*, 2014, **5**, 3853–3858.

22 (*a*) P. Cui, M. R. Hoffbauer, M. Vyushkova and V. M. Iluc, Heterobimetallic Pd–K Carbene Complexes via One-Electron Reductions of Palladium Radical Carbenes, *Chem. Sci.*, 2016, **7**, 4444–4452; (*b*) R. Shimokawa, Y. Kawada, M. Hayashi, Y. Kataoka and Y. Ura, Oxygenation of a Benzyl Ligand in SNS-Palladium Complexes with O$_2$: Acceleration by Anions or Brønsted Acids, *Dalton Trans.*, 2016, **45**, 16112–16116; (*c*) Y. Shigehiro, K. Miya, R. Shibai, Y. Kataoka and Y. Ura, Synthesis of Pd-NNP Phosphoryl Mononuclear and Phosphinous Acid-Phosphoryl-Bridged Dinuclear Complexes and Ambient Light-Promoted Oxygenation of Benzyl Ligands, *Organometallics*, 2022, **41**, 2810–2821.

23 S. Min, J. Choi, C. Yoo, P. M. Graham and Y. Lee, Ni(0)-Promoted Activation of Csp^2–H and Csp^2–O Bonds, *Chem. Sci.*, 2021, **12**, 9983–9990.

24 We used $^{t\mathrm{Bu}}$MgCl instead of ^{t}BuLi for safety reasons.

25 In the ESI† we also describe attempts to prepare (^{t}BuPBP)Pd(allyl).

26 Y. Segawa, M. Yamashita and K. Nozaki, Syntheses of PBP Pincer Iridium Complexes: A Supporting Boryl Ligand, *J. Am. Chem. Soc.*, 2009, **131**, 9201–9203.

27 H. Ogawa and M. Yamashita, Platinum Complexes Bearing a Boron-Based PBP Pincer Ligand: Synthesis, Structure, and Application as a Catalyst for Hydrosilylation of 1-Decene, *Dalton Trans.*, 2013, **42**, 625–629.

28 For selected references see: (*a*) H.-W. Suh, T. J. Schmeier, N. Hazari, R. A. Kemp and M. K. Takase, Experimental and Computational Studies of the Reaction of Carbon Dioxide with Pincer-Supported Nickel and Palladium Hydrides, *Organometallics*, 2012, **31**, 8225–8236; (*b*) H.-W. Suh, D. Balcells, A. J. Edwards, L. M. Guard, N. Hazari, E. A. Mader, B. Q. Mercado and M. Repisky, Understanding the Solution and Solid-State Structures of Pd and Pt PSiP Pincer-Supported Hydrides, *Inorg. Chem.*, 2015, **54**, 11411–11422.

29 An alternative route involving the use of 1,4-dioxane as an additive is described in the ESI†

30 (*a*) A. J. Canty, N. J. Minchin, B. W. Skelton and A. H. White, Cyclopalladation to Form Planar Tridentate [N–C–N]–Intramolecular Co-ordination Systems Involving Pyridine Donor Groups, Including Ligand Synthesis and X-ray

Structural Studies, *J. Chem. Soc., Dalton Trans.*, 1987, 1477–1483; (*b*) M. Bröring, C. Kleeberg and E. Cónsul Tejero, Syntheses, Structures and Coordination Modes of Acetatopalladium(II) Complexes with 1,3-Bis(2-arylimino)isoindoline Ligands of Different Steric Influence, *Eur. J. Inorg. Chem.*, 2007, 3208–3216; (*c*) C. M. Anderson, N. Oh, T. A. Balema, F. Mastrocinque, C. Mastrocinque, D. Santos, M. W. Greenberg and J. M. Tanski, Regioselective C–H/C–X Activation of Naphthyl-Derived Ligands to Form Six-Membered Palladacycles, *Tetrahedron Lett.*, 2016, **57**, 4574–4577; (*d*) M. R. Hoffbauer, C. C. Comanescu, B. J. Dymm and V. M. Iluc, Influence of the Leaving Group on C–H Activation Pathways in Palladium Pincer Complexes, *Organometallics*, 2018, **37**, 2086–2094.

31 A reviewer suggested that the presence of different halide salt impurities in variable concentrations may be causing the large changes in the rates of CO_2 insertion into **1-Me**, **1-Et**, and **1-^{n}Pr**. In the ESI,† we have described experiments that were performed to discount this possibility.

32 J. E. Heimann, W. H. Bernskoetter and N. Hazari, Understanding the Individual and Combined Effects of Solvent and Lewis Acid on CO_2 Insertion into a Metal Hydride, *J. Am. Chem. Soc.*, 2019, **141**, 10520–10529.

33 (*a*) C. Reichardt, Solvatochromic Dyes as Solvent Polarity Indicators, *Chem. Rev.*, 1994, **94**, 2319–2358; (*b*) C. Reichardt, Empirical Parameters of the Polarity of Solvents, *Angew. Chem., Int. Ed.*, 1965, **4**, 29–40.

34 The Dimroth-Reichardt $E_T(30)$ parameter is determined from the molar electronic transition energy of 2,6-diphenyl-4-(2,4,6-triphenylpyridinium-1-yl)phenolate (conventionally referred to as Betaine 30). It is found by measuring the λ_{max} of Betaine 30 in a particular solvent and a smaller λ_{max} corresponds to a larger wavenumber and therefore a more polar solvent.

35 (*a*) J. E. Heimann, W. H. Bernskoetter, N. Hazari and J. M. Mayer, Acceleration of CO_2 Insertion into Metal Hydrides: Ligand, Lewis Acid, and Solvent Effects on Reaction Kinetics, *Chem. Sci.*, 2018, **8**, 6629–6638; (*b*) J. E. Heimann, W. H. Bernskoetter, J. A. Guthrie, N. Hazari and J. M. Mayer, Effect of Nucleophilicity on the Kinetics of CO_2 Insertion into Pincer-Supported Nickel Complexes, *Organometallics*, 2018, **37**, 3649–3653.

36 T. Moragas, M. Gaydou and R. Martin, Nickel-Catalyzed Carboxylation of Benzylic C–N Bonds with CO_2, *Angew. Chem., Int. Ed.*, 2016, **55**, 5053–5057.

37 In the S_E2 pathway, we were unable to find the intermediate and barrier for the second rearrangement step to form the palladium carboxylate product, as the rearrangement occurs spontaneously during geometry optimization. However, this process has previously been demonstrated to be low energy in related systems.

38 The calculated increase in barrier from **1-Et** (17.7 kcal mol^{-1}) to **1-Me** (19.4 kcal mol^{-1}) is around 1 kcal mol^{-1} larger than would be expected for a two-fold difference in rate. Nevertheless, this is good agreement when computational error is considered.

39 L. Falivene, R. Credendino, A. Poater, A. Petta, L. Serra, R. Oliva, V. Scarano and L. Cavallo, SambVca 2. A Web Tool for Analyzing Catalytic Pockets with Topographic Steric Maps, *Organometallics*, 2016, **35**, 2286–2293.

40 D. García-López, L. Pavlovic and K. H. Hopmann, To Bind or Not to Bind: Mechanistic Insights into C–CO_2 Bond Formation with Late Transition Metals, *Organometallics*, 2020, **39**, 1339–1347.